Research Article Vol. 33, No. 25 / 15 Dec 2025 / Optics Express 52399
Optics EXPRESS

Design and construction of a high-efficiency linearly polarized Nd:YAG laser at 1064 nm using diode side-pumping in a coupled ring-linear cavity

MARYAM DANESHVARPOUR,[1,2] MOHAMMAD SABAEIAN,[1,2] AND ALLAN BERECZKI[3]

[1]Department of Physics, Faculty of Science, Shahid Chamran University of Ahvaz, Ahvaz 61357-83151, Iran
[2]Center for Research on Laser and Plasma, Shahid Chamran University of Ahvaz, Ahvaz 61357-83151, Iran
[3]Fuel Cell and Hydrogen Center, IPEN – São Paulo 05468-901, Brazil

Abstract: This study presents the design, modelling, and implementation of a high-efficiency, linearly polarized Nd:YAG laser operating at 1064 nm, based on what we believe to be a novel coupled ring–linear cavity configuration with diode side-pumping. To overcome the challenges of unpolarized emission and thermal lensing in side-pumped solid-state lasers, a side cavity containing a Brewster window was integrated, enabling quasi-unidirectional operation and enhanced polarization purity. A 50% increase in output power was achieved compared to the conventional ring cavity, while the polarization conversion efficiency reached up to 82%. The thermal lens focal length was characterized both experimentally and via LASCAD simulation, showing close agreement (e.g., 760 mm vs. 802 mm at 13 A). Comprehensive stability analysis using the ABCD matrix method and LASCAD simulations guided the optimization of cavity geometry, minimizing astigmatism and ensuring mode stability. Experimental validation demonstrated near-diffraction-limited beam quality with $M^2 \approx 1.2$, measured according to ISO 11146-1:2005. In addition, optimal positioning of the nonlinear crystal (99 mm from M4) was identified for efficient second harmonic generation. This coupled cavity strategy offers a robust and scalable solution for generating high-power, polarized beams in solid-state lasers, particularly benefiting applications in nonlinear optics, frequency conversion, and single-frequency operation.

1. Introduction

The configuration of a laser resonator is a critical factor in determining its output characteristics. A resonator typically comprises a gain medium, reflective mirrors, and an output coupler, but additional components such as nonlinear crystals, polarizers, magneto-optic crystals, saturable absorbers, or optical isolators may be incorporated depending on the application. Common resonator configurations include linear, V-shaped, Z-shaped, X-shaped, and ring designs. In a linear (standing wave) configuration, light oscillates between the back and front mirrors, behaving as a standing wave. In a ring configuration, light travels in a closed path in both directions, with the option to eliminate one direction to achieve unidirectional operation. Unidirectional operation in a ring resonator is particularly important for frequency doubling, as it can significantly enhance efficiency. Compared to linear resonators, ring resonators offer several advantages: a stability range twice as wide, reduced sensitivity to misalignment, and more stable output with fewer fluctuations due to the elimination of bidirectional wave interference [1]. These configurations are selected based on the specific requirements of the laser system. For instance, ring resonators are preferred for unidirectional laser operation. Figure 1 illustrates a simplified schematic of a ring resonator.

#575625 https://doi.org/10.1364/OE.575625
Journal © 2025 Received 5 Aug 2025; revised 26 Aug 2025; accepted 26 Aug 2025; published 4 Dec 2025

Optics EXPRESS

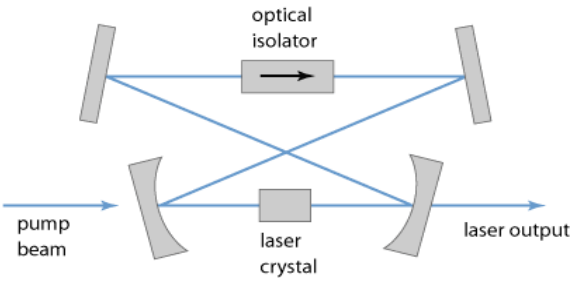

Fig. 1. Schematic design of a ring resonator.

Ring resonators are well-suited for achieving stable laser output with a narrow spectral linewidth and for single-frequency unidirectional lasers [2]. Their broader stability range compared to linear cavities allows for a larger beam waist within the crystal, which is particularly advantageous for side-pumped systems. The laser output power is proportional to the overlap between the pumped gain medium and the laser mode within the crystal, making a wide and stable beam waist highly desirable. Magni et al. demonstrated that to maintain a large mode volume while minimizing diffraction losses, the beam waist within the crystal should be 50–83% of the laser rod's radius [3]. In Nd:YAG crystals, achieving this ideal beam waist is challenging due to strong thermal lensing and losses from the unpolarized laser output. However, a ring resonator's wider stability range facilitates closer attainment of this goal.

Another critical consideration driving the adoption of ring resonators and unidirectional operation is the inherently unpolarized output of Nd:YAG lasers. Polarized laser beams are essential for applications such as second-harmonic generation (SHG), where phase-matching in nonlinear crystals like KTP depends on the polarization state of the input beam. To achieve unidirectional operation in ring resonators, optical isolators are commonly used, consisting of a polarizer (e.g., Brewster window or thin-film polarizer), a half-wave plate, and a magneto-optic crystal (e.g., TGG) in a permanent magnetic field. Therefore, to achieve a unidirectionally polarized laser suitable for critical applications such as SHG, it is necessary to introduce multiple components into the cavity, each of which can cause losses in the cavity. Hence, the idea of placing a side cavity alongside the main cavity can be beneficial in this regard.

The development of coupled cavity laser systems has significantly advanced laser performance across various applications. In 1990, Ursula Keller pioneered coupled-cavity designs for ultrafast lasers, introducing the semiconductor saturable absorber mirror (SESAM) for passive mode-locking in solid-state lasers like Ti:Sapphire and Nd:YLF, focusing on ultrashort pulse generation [4]. In 1993, He et al. explored coupled resonant cavities in Q-switched Nd:YAG lasers, achieving multiple mode-locking to control pulse repetition rates, demonstrating the versatility of cavity coupling for pulse dynamics [5]. By 1999, Deleva et al. developed a ring-linear coupled cavity for injection-seeded Nd:YAG lasers, emphasizing spectral purity and reverse-wave suppression for tunable systems [6]. Recent research has shifted toward microscale systems, with studies in 2015 by D'Agostino et al. and Cao et al. leveraging multimode interference and dielectric microcavities for tunable single-mode lasing and wave chaos studies, respectively [7,8]. In 2016, Sapingi's PhD thesis introduced coupled cavity lasers for biological cell analysis, focusing on microscale semiconductor systems [9]. In 2017, Bahari et al. utilized topological edge modes for nonreciprocal lasing in microcavities [10], and in 2021, Ullah et al. advanced single-mode nanowire lasers using coupled cavities for nano photonics [11]. In 2024, Gianfrani et al. reviewed cavity-enhanced spectroscopy, employing high-finesse cavities for precision measurements [12]. Most recently, in 2025, Letsou et al. demonstrated hybridized soliton lasing in coupled semiconductor ring lasers, generating complex frequency combs [13]. While recent

Optics EXPRESS

efforts focus on microscale and soliton-based systems, macroscale solid-state laser research, such as the high-efficiency, linearly polarized Nd:YAG laser with a ring-linear coupled cavity, remains distinct, building on Keller's foundational work but prioritizing power amplification and polarization control for applications like SHG.

In this study, we achieved quasi-unidirectional operation by integrating a side cavity at the laser output, incorporating a polarizer to produce a high-efficiency linearly polarized 1064 nm laser beam. By redirecting one of the laser beam paths back into the active medium, we were not only able to suppress cavity instability—characterized by continuous fluctuations in laser output power—but also significantly improved the efficiency of polarized beam generation relative to the total output power. Moreover, a high-quality laser output was achieved, with an M^2 value approaching 1.

2. LASCAD simulation

To gain insight into cavity dynamics, the ring cavity was simulated in LASCAD with distances and angles within the stability range LASCAD's specialized laser cavity design capabilities enabled accurate prediction of experimental outcomes. The laser module (GN75-H-3 × 78-CX-40, Oriental Laser, China) used in this setup has a maximum output power of 75 W and is water-cooled. The Nd:YAG crystal, with dimensions Ø3 mm × 78 mm and 0.6% doping, is side-pumped by 12 diodes in a triple configuration at 808 nm. Figure 2 shows a schematic view of the arrangement of diodes in three rows at an angle of 120 degrees around the crystal. Each row contains 4 diodes with a length of approximately 10 millimetres and a distance of 4 millimetres between the diodes. Side-pumping reduces thermal effects from focused pump beams along the crystal's axis and eliminates the need for precise pump beam focusing.

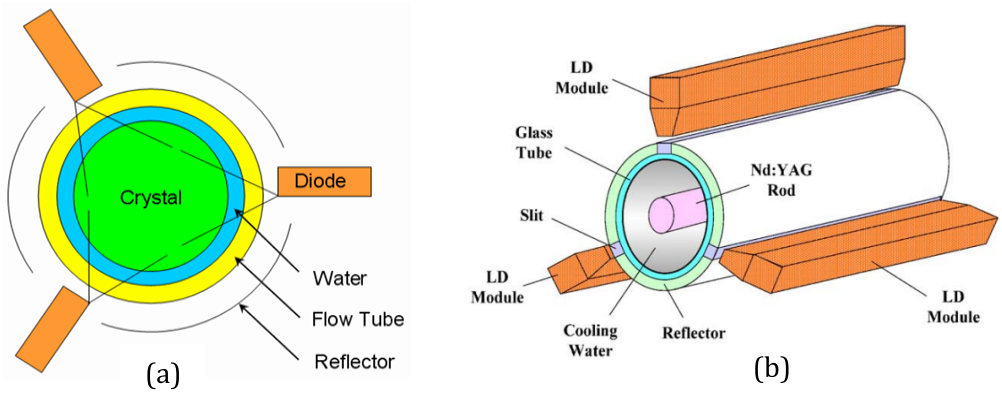

Fig. 2. Schematic view of the arrangement of diodes in three rows at an angle of 120 degrees around the crystal in side-pumped configuration: (a) Front view and (b) Side view. Each row contains 4 diodes with a length of approximately 10 mm and a distance of 4 mm between the diodes.

The simulated cavity is shown in Fig. 3. For this simulation, all important parameters such as the type, number and spacing of diodes, the type of cooling, all distances of mirrors and crystal have been accurately entered. This laser module employs twelve diodes arranged in a three-row array at an angle of 120 degrees around the crystal, emitting radiation at a wavelength of 808 nm. The level 0 is a flat mirror with high-reflectivity at 1064 nm (Mirror M1). The level 4 is a flat mirror with 15% transmission at 1064 nm (Mirror M2), serving as the output coupler. Levels 5,6 are curved mirrors with a 200 mm radius of curvature and high reflectivity at 1064 nm (Mirrors M3 and M4). levels 2 and 3 correspond to the beginning and end of the crystal.

Optics EXPRESS

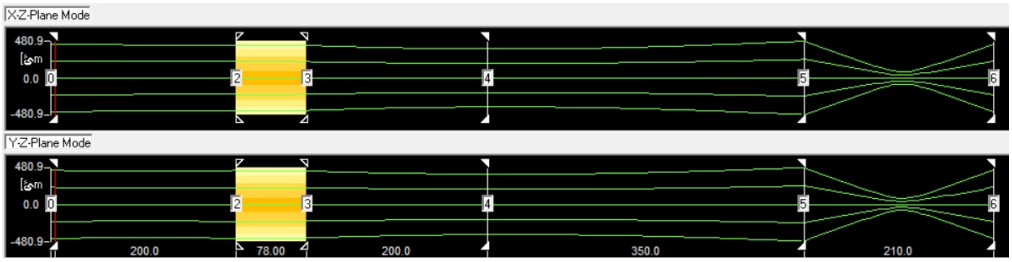

Fig. 3. Ring cavity designed in LASCAD, levels 0 and 4 correspond to flat mirrors M1 and M2, levels 5 and 6 correspond to mirrors M3 and M4, and levels 2 and 3 correspond to the beginning and end of the crystal, green lines indicate the resonance of the TEM00 mode in the cavity.

Finite element analysis (FEA) in LASCAD calculates critical parameters, including temperature distribution, output power, laser spot size across the cavity, thermal lens focal length, and mode profiles [14].

The temperature distribution (Fig. 4) showed a 2.5 K difference between the crystal's centre and surface, indicating effective cooling given Nd:YAG high thermal conductivity (14 W/m·K).

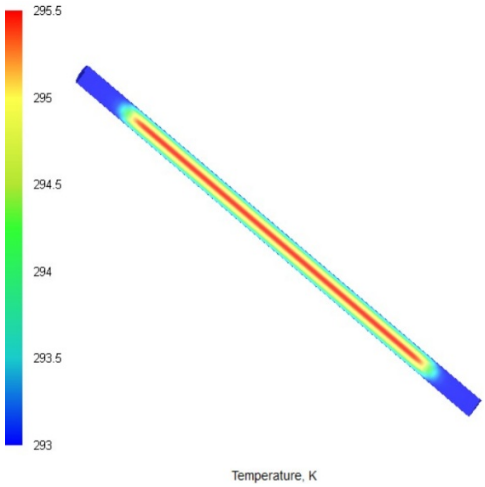

Fig. 4. Temperature distribution estimated by LASCAD showing a temperature difference of 2.5 K between the center of the crystal and the lateral surface.

Simulations provided insights into parameters difficult to measure experimentally. Table 1 lists calculated parameters, such as the optimal position for a nonlinear crystal (99 mm from M4) for frequency doubling, where the smallest spot size enhances nonlinear efficiency. The small difference in spot size between sagittal and tangential planes at the output coupler and focal point indicates low astigmatism, consistent with the use of small mirror angles. The spot size at the output (443 µm) and between M3 and M4 (78 µm) was calculated using TEM_{00} mode analysis, confirming cavity optimization for the fundamental mode. The thermal focal length at 13 A (802 mm) aligns with reported values (700–900 mm for side-pumped Nd:YAG) [14], validating the simulation's accuracy.

Optics EXPRESS

Table 1. Parameters calculated for the output of 1064 nm primary ring cavities by LASCAD at 13 A

Spot size on OC (TEM00) [μm]		The smallest Spot size between M3&M4 (TEM00) [μm]		Stability Criteria		Focal length of thermal Lens [mm]	
x-z Plane	y-z Plane	x-z Plane	y-z Plane	x-z Plane	y-z Plane	x-z Plane	y-z Plane
443	443.22	78.588	78.46	-0.31	-0.39	802.26	802.625

3. Experimental measurement of the thermal lense

The thermal focal length induced in side-pumped Nd:YAG was determined experimentally. This is done in two ways: non-lasing and lasing. In both cases, the He-Ne laser was passed through the crystal along its axis. The pump source was activated, and the focal point of the He-Ne beam was identified. As the current applied to the diode lasers increased, enhancing pump power, the thermal focal point moved closer to the crystal and became smaller [15]. Experimental focal lengths were measured in a non-lasing and lasing conditions, and potential human error was minimized using a beam profiler (A 3D beam profiler made by Parto Nameh Asha Iran, where we found the beam waist by moving the beam profiler sensor at a specific distance around the focal point) though slight discrepancies may persist. In the non-lasing state, we do not have any mirrors in the arrangement, but in the lasing state, front and rear mirrors are used to create resonance in the cavity. In fact, for this condition, we considered a linear arrangement. To prevent damage to the He-Ne laser, we applied a small angle to the passage of this laser beam through the crystal so that the laser produced in the cavity does not enter the He-Ne laser directly. Figure 5 shows the schematic design of these two conditions. The experimental results in non-lasing condition, indicate maximum and minimum focal lengths of approximately $f_{th,max} \approx 1700\ mm$ and $f_{th,min} \approx 600\ mm$, respectively (minimum focal length is at maximum current and maximum at threshold input current for start laser operation) and for lasing condition, $f_{th,max} \approx 1540\ mm$ and $f_{th,min} \approx 500\ mm$.

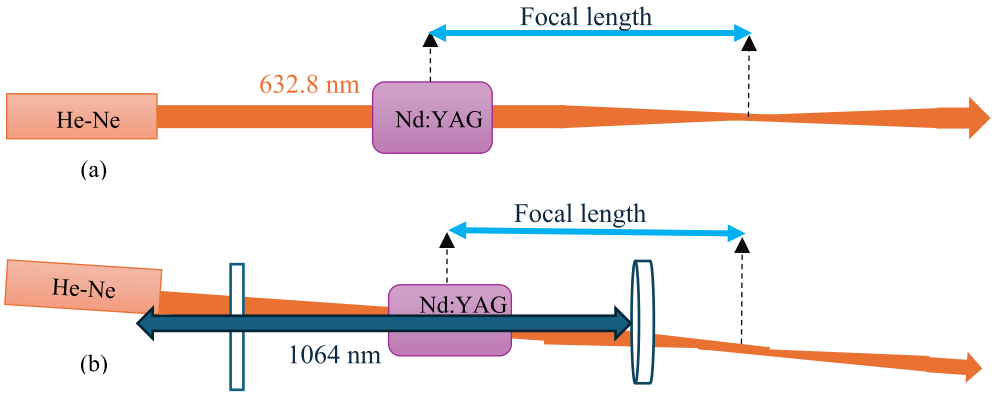

Fig. 5. Schematic design of non-lasing (a) and lasing (b) for experimental thermal focal length measurement. In lasing conditions, by applying a small angle to the He-Ne laser beam, we prevent the entry of the generated 1064 nm laser into it.

The thermal focal length, dependent on pump power (current of diodes), was simulated for the current range. Results are presented in Table 2 and plotted in Fig. 6, showing good agreement with experimental measurements and LASCAD simulation.

Optics EXPRESS

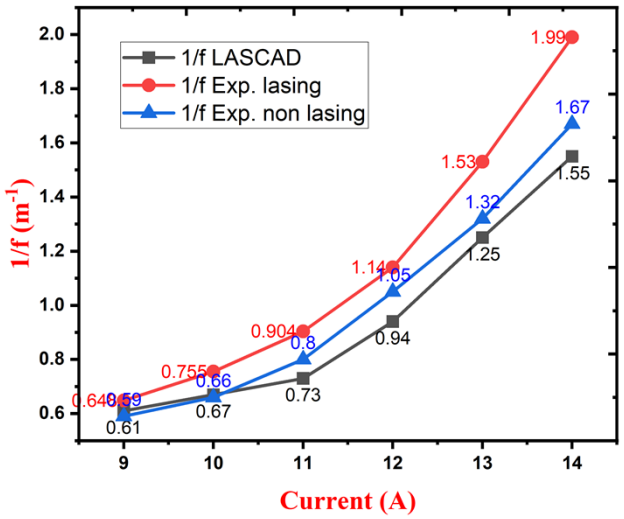

Fig. 6. Comparison of the diopter of the crystal thermal lens with LASCAD simulation and experimental method in two cases of lasing and nonlasing. Exp. stands for experimental.

Table 2. Thermal lens focal length calculated for the output of 1064 nm primary ring cavity by LASCAD simulation and experimental method

Thermal Focal Length [mm]					
Current [A]	Voltage [v]	x-z Plane	y-z Plane	Experimental (non lasing)	Experimental (lasing)
9	19.5	1646.65	1659.31	≈ 1680	≈ 1540
10	19.6	1493.77	1503.31	≈ 1520	≈ 1320
11	19.7	1367.00	1374.23	≈ 1300	≈ 1100
12	19.8	1066.05	1068.95	≈ 1020	≈ 880
13	19.9	802.26	802.63	≈ 760	≈ 650
14	20	643.79	643.19	≈ 600	≈ 500

The data indicates a clear trend: as the current increases, the focal length decreases, resulting in a corresponding increase in diopter values across two methods. This suggests a strengthening of the thermal lens effect with higher current, likely due to increased heat generation and thermal gradients within the crystal.

The LASCAD simulation (black squares) provides a baseline, with diopter values ranging from 0.61 A at 9 A to 1.55 A at 14 A, reflecting a moderate thermal lens effect. The experimental lasing condition (red circles), with values from 0.648 to 1.99, consistently shows higher diopters than the simulation, indicating a stronger thermal lens possibly due to additional heat from lasing activity. Conversely, the non-lasing experimental condition (blue triangles), ranging from 0.59 m^{-1} to 1.67 m^{-1}, exhibits the lowest diopter values, suggesting a weaker thermal lens effect in the absence of lasing-induced heating.

The focal length data (table) corroborates this trend, with lasing conditions yielding the shortest focal lengths (e.g., ~500 mm at 14 A) compared to non-lasing (~600 mm) and LASCAD (~643 mm), highlighting the influence of lasing on thermal lensing. These findings suggest that lasing amplifies the thermal lens effect, which could impact laser cavity design and stability, necessitating further investigation into heat dissipation and material properties under operational conditions.

Optics EXPRESS

4. Stability analysis using the ABCD matrix method

In addition to simulation, the ABCD matrix method is a common and effective approach for calculating and analysing certain cavity parameters. To initiate the experimental setup, key parameters such as cavity stability, laser spot size, and the stability range for variations in element spacing were calculated using the ABCD matrix method. The matrices used for all optical elements are listed in Table 3.

Table 3. Matrix of elements used in cavity [16]

Optical element	ABCD Matrix	Description of the parameters
Free Space	$\begin{pmatrix} 1 & d \\ 0 & 1 \end{pmatrix}$	d is the length of free space.
Mirror	Sagittal Plane: $\begin{pmatrix} 1 & 0 \\ \frac{-2\cos\theta}{R} & 1 \end{pmatrix}$ Tangential Plane: $\begin{pmatrix} 1 & 0 \\ \frac{-2}{R\cos\theta} & 1 \end{pmatrix}$	R is the radius of the curvature of the mirror and θ is the angle of incidence of the beam.
Crystal	$\begin{pmatrix} 1 & \frac{l}{n} \\ 0 & 1 \end{pmatrix}$	l and n are the length and refractive index of the crystal respectively.
Thermal lens of the crystal	$\begin{pmatrix} 1 & 0 \\ \frac{-1}{f_{th}} & 1 \end{pmatrix}$	f_{th} is the focal length of the crystal thermal lens.

The overall round-trip matrix in the ring setup of Fig. 7 for the two Sagittal and Tangential planes is given in Eqs. (1) and (2) as:

$$M_{round\_trip(t)} = \begin{pmatrix} 1 & 0 \\ \frac{-1}{f_{th}} & 1 \end{pmatrix}\begin{pmatrix} 1 & d_2+\frac{l}{2n} \\ 0 & 1 \end{pmatrix}\begin{pmatrix} 1 & d_5 \\ 0 & 1 \end{pmatrix}\begin{pmatrix} 1 & 0 \\ \frac{-2}{R\cos\theta} & 1 \end{pmatrix}\begin{pmatrix} 1 & d_4 \\ 0 & 1 \end{pmatrix}\begin{pmatrix} 1 & 0 \\ \frac{-2}{R\cos\theta} & 1 \end{pmatrix}\begin{pmatrix} 1 & d_3 \\ 0 & 1 \end{pmatrix}\begin{pmatrix} 1 & d_1+\frac{l}{2n} \\ 0 & 1 \end{pmatrix} \quad (1)$$

$$M_{round\_trip(s)} = \begin{pmatrix} 1 & 0 \\ \frac{-1}{f_{th}} & 1 \end{pmatrix}\begin{pmatrix} 1 & d_2+\frac{l}{2n} \\ 0 & 1 \end{pmatrix}\begin{pmatrix} 1 & d_5 \\ 0 & 1 \end{pmatrix}\begin{pmatrix} 1 & 0 \\ \frac{-2\cos\theta}{R} & 1 \end{pmatrix}\begin{pmatrix} 1 & d_4 \\ 0 & 1 \end{pmatrix}\begin{pmatrix} 1 & 0 \\ \frac{-2\cos\theta}{R} & 1 \end{pmatrix}\begin{pmatrix} 1 & d_3 \\ 0 & 1 \end{pmatrix}\begin{pmatrix} 1 & d_1+\frac{l}{2n} \\ 0 & 1 \end{pmatrix} \quad (2)$$

In choosing the order of the matrices, we started from the centre of the active medium and assumed that a thermal lens with focal length f_{th} is induced within it. After one round trip, the beam returns to the same initial point.

Table 4 presents the selected distances, parameters, and computed values using the ABCD matrix method. In the matrix method, after multiplying all the matrixes in a round trip, the final matrix will be a 2×2 matrix (M_{round_trip}):

$$M_{round\_trip} = \begin{pmatrix} A & B \\ C & D \end{pmatrix} \quad (3)$$

$$Stability\_condition = -1 < \left|\frac{A+D}{2}\right| < 1 \quad (4)$$

$$\omega = \sqrt{\frac{\lambda.B}{\pi.\sqrt{1-\left(\frac{A+D}{2}\right)^2}}} \quad (5)$$

Using the Eqs. (3)-(5) [17], we can calculate the cavity stability (Which must be between 1 and -1 for the cavity to be stable) and the laser spot size at any point of the cavity we want (we just need to start the round trip and matrix multiplication from our desired point). All matrix calculations were performed separately for two different $f_{th,max} = 1540\ mm$ and $f_{th,min} = 500mm$ cases in a lasing state and the results are shown in Table 4.

Optics EXPRESS

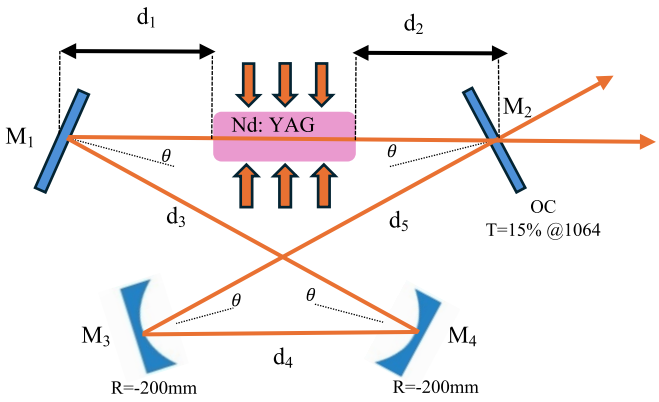

Fig. 7. Designed ring setup: M1 is a high reflectance mirror at 1064 nm, M2 is an output mirror with 15% transmission, and M3 and M4 are curved mirrors with 200 mm radius of curvature. The distance from M1 and M2 to the crystal is 200 mm (d_1, d_2), The distance between M_1-M_4 and M_2-M_3 is 350 mm at the arms (d_3, d_5), and the distance between two curved mirrors is 210 mm (d_4) that were calculated for optimal stability.

Table 4. Selected and calculated parameters using the ABCD matrix method

Constant parameters			*Calculated parameters by ABCD Matrix*							
$d_1 = d_2$	*Distance from M1&M2 to crystal*	*200 mm*	***Sagittal Plane***				***Tangential Plane***			
$d_3 = d_5$	*Diagonal arms*	*350 mm*	*ω (Spot size)*		*Stability*		*ω (Spot size)*		*Stability*	
d_4	*Distance between M3&M4*	*210 mm*	$For f_{th,max}$	$For f_{th,min}$	$For f_{th,max}$	$For f_{th,min}$	$For f_{th,max}$	$For f_{th,min}$	$For f_{th,max}$	$For f_{th,min}$
$f_{th,max}$	*Maximum of* f_{th}	*1540 mm*	*0.504 mm*	*0.766 mm*	*-0.101*	*0.908*	*0.485 mm*	*0.769 mm*	*-0.02*	*0.918*
$f_{th,min}$	*Minimum of* f_{th}	*500 mm*								
n	*Nd:YAG Refractive index*	*1.82*								
l	*crystal length*	*78 mm*								
R	*Radius of curvature of mirror M3,M4*	*-200 mm*								
θ	*the angle of incidence of the beam.*	*6°*								

The results show negligible astigmatism in the system, as evidenced by the small difference in spot size between the two planes. Maximum and minimum values in Table 4 correspond to the maximum and minimum thermal focal lengths, respectively. With these parameters, the experimental setup was established. The computational results indicate that as the thermal lens becomes stronger ($f_{th,min}$), the laser spot size within the crystal increases. Given that in a

Optics EXPRESS

side-pumped system, if the laser spot size in the crystal is approximately 50-83% of the crystal radius, higher-order mode resonances are suppressed, and the system approaches single-mode operation. Consequently, it can be expected that at higher currents, the system will tend toward single-mode behavior [3].

5. Experimental setup

5.1. Main ring cavity

With the simulation ran and stability calculations, we are now ready to set up the cavity. The ring resonator was configure as shown in Fig. 7. Mirror M1 is a flat with high-reflectivity at 1064 nm to minimize cavity losses. Mirror M2 is a flat mirror with 15% transmission at 1064 nm, serving as the output coupler to balance output power and cavity stability. Mirrors M3 and M4 are curved mirrors with a 200 mm radius of curvature and high reflectivity at 1064 nm, essential for focusing the laser beam for nonlinear crystal, which will be placed later, and maintaining cavity stability. To minimize astigmatism, the angle of incidence on the mirrors was set to 6 degrees, a practical choice that introduces negligible astigmatism while being feasible to implement. Astigmatism in ring cavities arises from differences in effective focal lengths of tilted mirrors which are different in sagittal and tangential planes, as described by Eq. (6):

$$f_t = \frac{f}{\cos\theta}, f_s = f.\cos\theta \tag{6}$$

where θ is the angle of incidence in radians, and f is the mirror's focal length [18]. Additionally, Eq. (7) shows that angled reflections introduce phase differences between the sagittal and tangential planes, contributing to astigmatism, though small angles minimize this effect [18]:

$$\triangle\varphi = \frac{\theta^2}{2R} \tag{7}$$

where R is the mirror's radius of curvature. All distances and angles were calculated using the ABCD matrix method in a home-made code and simulated in LASCAD to ensure stability and thermal optimization before implementation. Distances include 200 mm from M1 to the crystal's edge, 200 mm from M2 to the crystal's edge, 210 mm between M3 and M4, and 350 mm for the diagonal arms, forming a symmetric cavity. This configuration produced a 1064 nm laser in both clockwise and counterclockwise directions (clockwise and counterclockwise directions are considered in the lower part of the cavity where the curved mirrors are).

5.2. Side cavity

To achieve quasi-unidirectional operation, a coupled side cavity was implemented in two steps. *First step*, a high-reflectivity mirror at 1064 nm was used to reflect the clockwise output back into the cavity, requiring precise alignment to avoid damage (Fig. 8(a)). This increased output power and reduced power fluctuations. Before placing this mirror, the output laser had severe fluctuations in power, which were largely eliminated by placing this feedback mirror. The location of the feedback mirror is very important. This mirror should be placed at the image of the focal point between the two curved mirrors because this is the point where the wavefront is flat and we can be sure that if the feedback mirror is placed at the image of this point, the shape of the wavefront will not be distorted. This is also the point where the beam waist size is at its smallest and it is very important that the image of this point is not distorted for the phase matching of our nonlinear crystal (the nonlinear crystal will be located at the focal point between the two curved mirrors). Therefore, using the ABCD matrix method and a round-trip path (black arrows) as shown in the Fig. 8(a), we can find the exact location of the feedback mirror. *Second step*, an additional output coupler (OC2) with 40% transmission was placed in

Optics EXPRESS

the counterclockwise output path (Fig. 8(b)), reducing the total system transmission to 6% and further increasing output power by approximately 50% compared to the main ring cavity. One of the fundamental challenges in this setup is the incorporation of polarizing elements such as a Brewster window (BW) or thin-film polarizer (TFP). The polarization of the output beam is critical because when using a nonlinear crystal for frequency conversion, the phase matching of certain nonlinear crystals (e.g., KTP) depends on the polarization direction of the fundamental laser beam. Thus, the Nd:YAG laser must be polarized to ensure the nonlinear crystal operates under phase-matching conditions, thereby achieving high conversion efficiency [19].

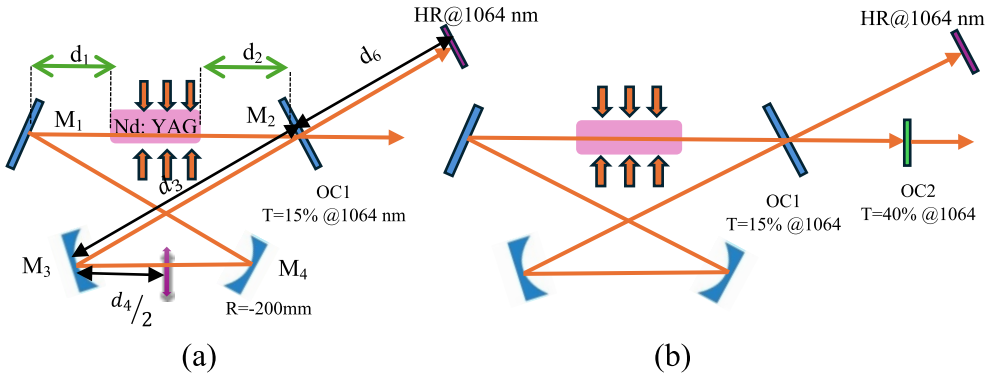

Fig. 8. (a) The location of the feedback mirror by using ABCD method, (b) add output coupler OC2 with 40% transmission placed in the counterclockwise output path.

To obtain the distance at which the spot size is equal to the spot size between the two curved mirrors, we use the parameter q. This parameter is defined as follows:

$$\frac{1}{q(z)} = \frac{1}{R(z)} - i\frac{\lambda}{\pi\omega^2(z)} \tag{8}$$

Where z is the position along the propagation axis, R(z) is the radius of curvature of the wavefront, ω(z) is the beam radius at that point and λ is the wavelength of the laser light. The imaginary part of this parameter gives the spot size. The round-trip matrix (black arrows in Fig. 8(a)) is obtained with Eqs. (9) and (10). Since, using LASCAD, we have the beam waist size at the focus between the two curved mirrors (ω_0 using Table 1), we can use the following relations to find the point where the beam waist size for a given d_6 is exactly equal to the beam waist size at the focus between the two curved mirrors:

$$M_{round\_trip(t)} = \begin{pmatrix} 1 & \frac{d_4}{2} \\ 0 & 1 \end{pmatrix}\begin{pmatrix} 1 & 0 \\ \frac{-2}{R\cos\theta} & 1 \end{pmatrix}\begin{pmatrix} 1 & d_3 \\ 0 & 1 \end{pmatrix}\begin{pmatrix} 1 & d_6 \\ 0 & 1 \end{pmatrix}\begin{pmatrix} 1 & d_6 \\ 0 & 1 \end{pmatrix}\begin{pmatrix} 1 & d_3 \\ 0 & 1 \end{pmatrix}\begin{pmatrix} 1 & 0 \\ \frac{-2}{R\cos\theta} & 1 \end{pmatrix}\begin{pmatrix} 1 & \frac{d_4}{2} \\ 0 & 1 \end{pmatrix} \tag{9}$$

$$M_{round\_trip(s)} = \begin{pmatrix} 1 & \frac{d_4}{2} \\ 0 & 1 \end{pmatrix}\begin{pmatrix} 1 & 0 \\ \frac{-2\cos\theta}{R} & 1 \end{pmatrix}\begin{pmatrix} 1 & d_3 \\ 0 & 1 \end{pmatrix}\begin{pmatrix} 1 & d_6 \\ 0 & 1 \end{pmatrix}\begin{pmatrix} 1 & d_6 \\ 0 & 1 \end{pmatrix}\begin{pmatrix} 1 & d_3 \\ 0 & 1 \end{pmatrix}\begin{pmatrix} 1 & 0 \\ \frac{-2\cos\theta}{R} & 1 \end{pmatrix}\begin{pmatrix} 1 & \frac{d_4}{2} \\ 0 & 1 \end{pmatrix} \tag{10}$$

Using Eqs. (11) to (14) and also the elements of the ABCD matrix that we obtained in Eqs. (9) and (10) and having the value of ω_0 using LASCAD, we can obtain the value of d_6:

$$q_{in} = i\pi\frac{\omega_0^2}{\lambda} \tag{11}$$

$$q_{out} = \frac{A.q_{in} + B}{C.q_{in} + D} \tag{12}$$

Optics EXPRESS

$$Z = \mathrm{Re}(q_{out}), Z_R = \mathrm{Im}(q_{out}) \tag{13}$$

$$\omega = \omega_0 \sqrt{1 + \left(\frac{Z}{Z_R}\right)^2} \tag{14}$$

With this method, we obtained the value of $d_6 = 240$ mm and based on this, we designed the side cavity. We also performed the same steps to calculate the location of OC2 and finally we set up the side cavity.

However, integrating a BW directly into the main cavity introduces two significant issues: (1) it causes beam deviation, necessitating realignment of the mirrors (of course, this can be fixed by re-adjusting the mirrors), and (2) it induces substantial power loss in the laser output (part of the power loss is due to laser polarization by BW, because ideally, each of the s- and p-polarization has 50% of the laser power also the power loss may be due to the depolarization losses. The problem consists in the radial and tangential induced birefringence that may depolarize part of the radiation that is subsequently be rejected by the polarizer). In this study, we mitigated these problems by strategically placing the BW in the side cavity, significantly reducing both beam misalignment and power attenuation while maintaining efficient polarization control. Figure 9 illustrates BW into the side cavity.

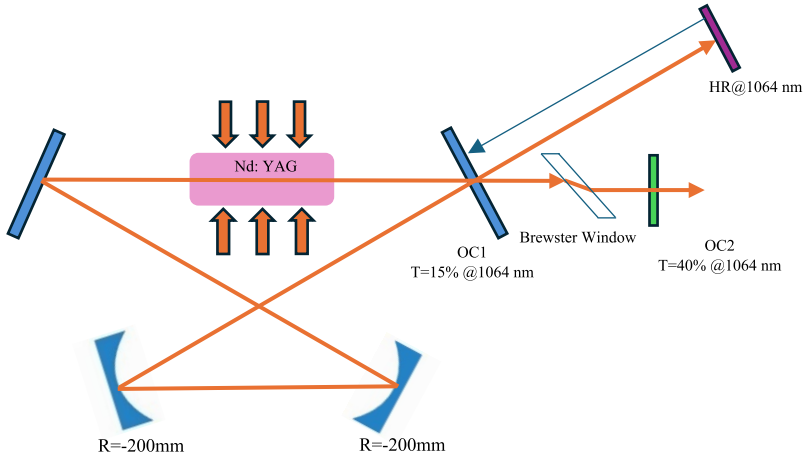

Fig. 9. Inserting the Brewster window into the side cavity.

6. Experimental results

6.1. Laser output power

To evaluate the impact of the coupled cavity on output power and polarization conversion efficiency, five configurations were tested. In the first case, a power meter was placed after OC1 (Fig. 10) to measure both clockwise and counterclockwise outputs (no OC2, HR mirror, or BW), denoted as *bidirectional power*. In the second case, a plane HR mirror at 1064 nm was placed in the clockwise output path, with the power meter between OC1 and OC2 (no OC2 or BW), denoted as *unidirectional power*. In the third case, OC2 with 40% transmission was added to the counterclockwise path, completing the side cavity, and the output power from OC2 was measured as *side cavity power*. In the fourth case, a BW was placed between OC1 and OC2 at the Brewster angle ($\theta_B = 56°$), with the power meter after OC2, denoted as *polarized side cavity power*. In the fifth case, to ensure that the output beam is polarized, a polarizing beam splitter (PBS) separated

Optics EXPRESS

the S- and P-polarizations, and the power meter measured the P-polarized output after the PBS, denoted as *p-polarized output*.

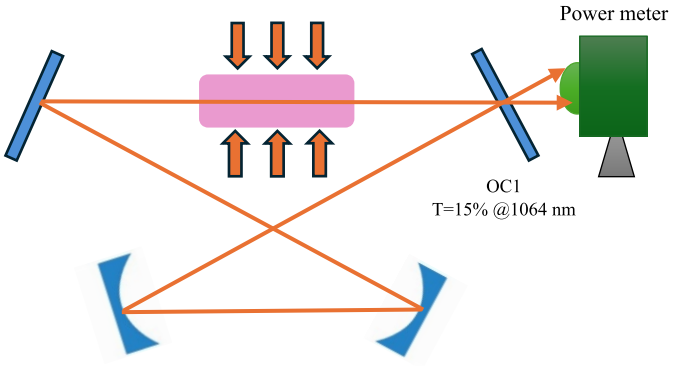

Fig. 10. The power meter is placed after OC1 to measure both clockwise and counterclockwise outputs.

The key metric is the conversion efficiency from unpolarized to polarized light, calculated as $\frac{\text{p\_polarized output power}}{\text{Side cavity power}}$, indicating the efficiency of producing polarized output. Since S- and P-polarizations of Nd:YAG lasers are initially equal, a 50% P-polarized output is expected, but the side cavity BW increased this efficiency. The ratio $\frac{\text{Side cavity power}}{\text{Bidirectional power}}$ reflects the power increase due to the side cavity. The side cavity not only boosted output power but also reduced the lasing threshold from 11 A to 7.5 A (The reduction in laser threshold is due to the reduction in the transmission percentage at the output mirror). Results are summarized in Table 5 and Fig. 11.

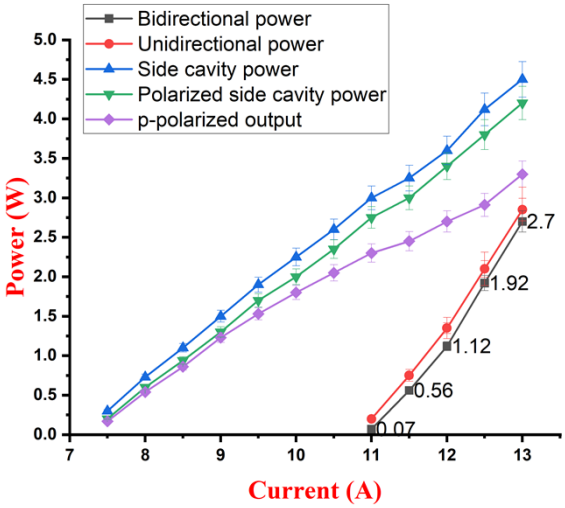

Fig. 11. Comparison of laser output power in five different cases given in Table 5.

The addition of the side cavity significantly enhanced the laser's performance, as evidenced by the data in Table 5. Comparing the bidirectional power (no side cavity) to the side cavity power, we observe a substantial increase in output power. For instance, at a current of 11 A, the bidirectional power is 0.07 W, while the side cavity power reaches 3 W. Similarly, at 12.5 A, the bidirectional power is 1.92 W, while the side cavity power is 4.12 W. The ratio $\frac{\text{Side cavity power}}{\text{Bidirectional power}}$

Optics EXPRESS

Table 5. Power measurement in different cases for polarized and non-polarized output

Current [A]	Bidirectional power [w]	Unidirectional power [w]	Side cavity power [w]	Polarized side cavity power [w]	P-polarized output [w]	$\frac{p\_polarizedoutputpower}{\text{Side cavity power}}$ %
7.5	-	-	0.3	0.2	0.17	57%
8	-	-	0.73	0.6	0.54	74%
8.5	-	-	1.1	0.94	0.86	78%
9	-	-	1.5	1.3	1.23	82%
9.5	-	-	1.9	1.7	1.53	81%
10	-	-	2.25	2	1.8	80%
10.5	-	-	2.6	2.35	2.05	79%
11	0.07	0.2	3	2.75	2.3	77%
11.5	0.56	0.75	3.25	3	2.45	75%
12	1.12	1.35	3.6	3.4	2.7	75%
12.5	1.92	2.1	4.12	3.8	2.91	71%
13	2.7	2.85	4.5	4.2	3.3	73%

consistently shows that the side cavity amplifies the output power across all measured currents. In the single ring cavity configuration (bidirectional power), the laser is unpolarized, with S- and P-polarizations being equal, resulting in an expected 50% P-polarized output. However, with the coupled cavity (including the side cavity and Brewster window), both the output power and polarization conversion efficiency are significantly improved. The polarization conversion efficiency, defined as $\frac{\text{p\_polarized output power}}{\text{Side cavity power}}$, ranges from 57% at 7.5 A to a peak of 82% at 9 A, as shown in Table 5. This is a marked improvement over the 50% baseline of the single ring cavity, demonstrating that the coupled cavity not only boosts output power but also enhances the efficiency of producing polarized light, with values consistently above 70% for currents of 8 A and higher. According to Table 5, the polarization conversion efficiency increased from 57% at 7.5 A to 82% at 9 A, likely due to better gain medium saturation and improved mode-pump overlap at higher currents. However, at 13 A, efficiency dropped to 73%, possibly due to stronger thermal lensing and increased diffraction losses, consistent with Magni et al.'s findings on pump power's impact on mode stability [2]. Overall, a 70% efficiency in converting unpolarized 1064 nm light to polarized light was achieved, a significant result for further applications.

6.2. Degree of polarization (DOP) in the main ring cavity

One of our goals for designing a side cavity is to be able to place the polarizer, here a Brewster window (BW), outside the main cavity, and we have three important reasons for doing this. *First*, the deflection that the BW creates in the beam path requires us to move and re-adjust the mirrors, which would be much easier to control if we placed the BW in the side cavity. *Second*, measurements show that in general the BW reduces the power by about 50% (due to the elimination of one polarization), but in the case where we placed this component in the side cavity, the efficiency of converting unpolarized to polarized beam was about 70%, which imposes less loss on the system (Table 5). In addition to polarization efficiency, the degree of polarization of the beam is of great importance to us. Therefore, as we will see later, we calculated the degree of polarization using the leakage of the main ring cavity mirrors. Therefore, *the third* reason demonstrating the advantage of the side cavity is the achievement of an appropriate degree of polarization for the laser beam within the main cavity. Since we did not have access to the main laser beam in the main cavity, using the leakage of the mirrors is a logical way to ensure proper polarization of the laser beam inside the ring cavity. it is important for us that the laser beam is

Optics EXPRESS

polarized to the appropriate degree in the ring cavity. To measure the degree of polarization, we used the leakage of curved mirrors as shown in the Fig. 12. For this purpose, we used a PBS cube to separate the S- and P-polarizations and measured both directions using two power meters (Table 6) and then calculated the degree of polarization using the Eq. (15) [20]. This was done both for the leakage of the curved mirrors to measure the degree of polarization inside the ring and for the final output from the side cavity. Because the amount of laser leakage from curved mirrors is very weak, we used a sensitive power meter for measurement, which is why the power values in the table for this case are expressed in milliwatts. The results are shown in Table 6 and Fig. 13.

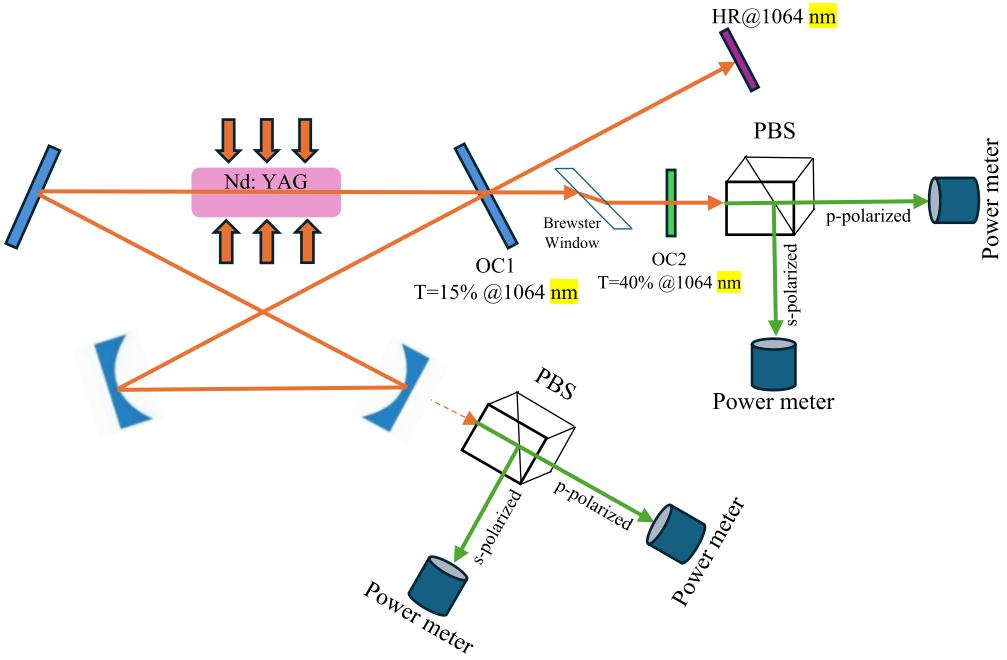

Fig. 12. Measuring DOP using the leakage of curved mirror for main ring cavity and for final output from OC2.

Table 6. The measurement of DOP for main cavity and final output.

For main ring cavity				For final output from OC2		
Current [A]	P_{max} $[mW]$	$P_{min}[mW]$	DOP	$P_{max}[W]$	$P_{min}[W]$	DOP
8	0.7	0.1	75%	0.12	0.03	60%
8.5	1.7	0.2	79%	0.3	0.07	62%
9	3.8	0.6	73%	0.58	0.17	55%
9.5	4	0.7	70%	0.69	0.22	52%
10	5.8	1	71%	1.1	0.3	57%
10.5	8.6	1.1	77%	1.53	0.37	61%
11	11	1.3	79%	1.95	0.47	61%
11.5	12	1.6	76%	2.18	0.75	49%
12	14.5	2.3	73%	2.77	0.97	48%

Optics EXPRESS

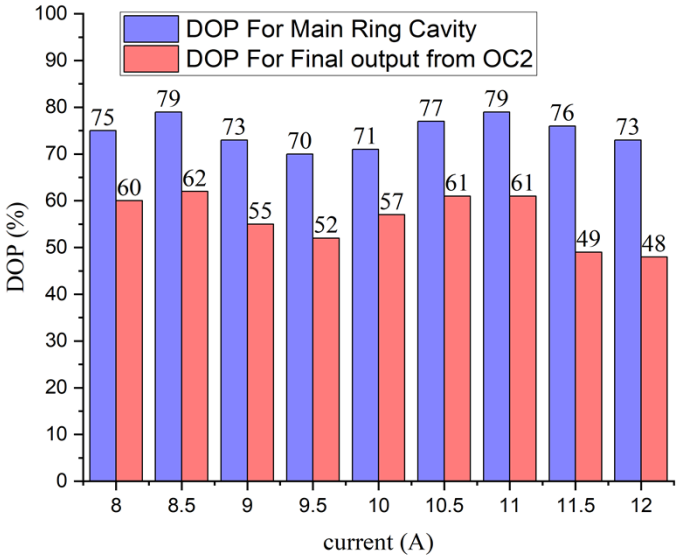

Fig. 13. Comparison between DOP for main cavity and final output.

We considered the output power from PBS in the direct direction as the maximum power and the output power in the perpendicular direction as the minimum power, which are shown in this regard as P_{max} and P_{min} respectively.

$$DOP(\%) = \left(\frac{P_{\max} - P_{\min}}{P_{\max} + P_{\min}}\right) \times 100 \tag{15}$$

Our calculations and measurements, as shown in the Fig. 13, show that by placing the BW in the side cavity, the degree of polarization of the laser beam in the main cavity not only has a suitable value (above 70%), but also the degree of polarization of the laser beam that we get from the side cavity as the final output is even higher (Table 6). Therefore, it seems that not only does the side cavity perform the polarization operation correctly, but by creating a polarized beam and reinjecting it into the main cavity, it will also enhance the polarization degree in the main cavity, i.e., it is as a polarized laser seed enters the ring cavity. In fact, the laser beam exiting OC1 is polarized by the BW upon re-resonance in the side cavity and returns to the ring cavity again, but this time it is polarized in a specific direction, during resonance in the ring cavity, this polarization direction is amplified and the degree of polarization inside the ring is greater than that exiting the side cavity.

6.3. Determination of the M^2 factor

The M^2 factor, also known as the beam propagation factor or beam quality parameter, is a widely used metric to quantify the quality of a laser beam by describing how well it can be focused or propagated compared to an ideal Gaussian beam. Introduced by Siegman in 1990, the M^2 factor provides a measure of a beam's divergence and spatial coherence, critical for applications in laser optics, such as material processing, telecommunications, and scientific research [21]. This dimensionless parameter relates the intensity distribution at the beam waist to that in the far field, providing insight into the beam's deviation from ideal Gaussian behavior. The knowledge of this factor is often necessary for laser system designers so as to control the quality of generated beams and compare them to standard ones. It is defined as the ratio of the beam parameter product (BPP) of the actual beam to that of a diffraction-limited Gaussian beam with the same waist size.

Optics EXPRESS

The parameters are shown in schematic Fig. 14. A M^2 value of 1 indicates a perfect Gaussian beam, while higher values indicate deviations from ideal behavior due to factors like aberrations or multi-mode operation [22]. The M^2 factor is standardized in the ISO 11146 series, which outlines methods for measuring beam widths, divergence angles, and the M^2 parameter [23].

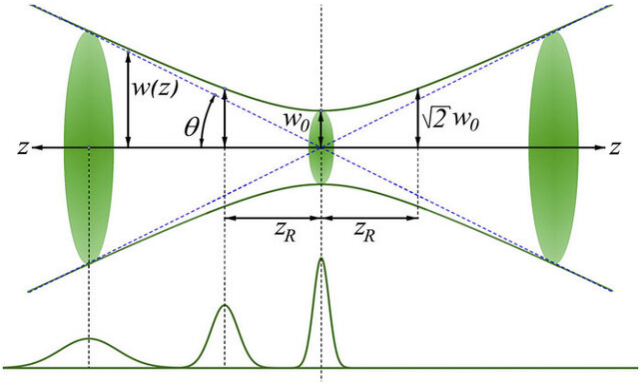

Fig. 14. The schematic display of the beam emission and the corresponding parameters including beam waist (ω_0), Rayleigh range (Z_R), and divergence angle (θ).

The ISO-based method is, indeed, the most commonly used one for the calculation of laser parameters such as beam width, divergence angle, and beam quality factor. Through this method, an optical arrangement, Fig. 16, is used to record the beam diameter at different points on a z-axis. Since the variation of laser beam emission is approximately hyperbolic, the data are processed through a hyperbolic equation of:

$$\omega^2(z) = A + Bz + Cz^2 \tag{16}$$

First, the geometrical indices A, B, and C were calculated by means of a home-made code written in the Maple programming and then based on the following equations, the M^2 factor, the divergence angle (θ), the Rayleigh length (Z_R), and the focal depth (b) were calculated:

$$M^2 = \frac{\pi}{4\lambda}\sqrt{AC - \frac{B^2}{4}} \tag{17}$$

$$\theta = \sqrt{C} \tag{18}$$

$$Z_R = \frac{1}{2C}\sqrt{4AC - B^2} \tag{19}$$

$$b = 2Z_R \tag{20}$$

The Rayleigh length suggests how far from the beam centre the beam light remains parallel [20]. In our experimental method, to calculate the M^2 quality factor, a beam profiler and a lens with a focal length of 25 mm were used (Fig. 16). The focal point of the laser beam was determined and designated as z = 0. Subsequently, by selecting 1 mm intervals on both sides of the focal point along the z-axis, the beam profiler was moved to measure beam parameters, including the spot size in the x and y directions and the full width at half maximum (FWHM) along these axes at all points. The graph of the obtained points and the quadratic function fitted to them is shown in the Fig. 15.

Using a custom-written code and applying a second-order polynomial fit, the coefficients A, B, and C were obtained. The desired parameters, particularly M^2, were then calculated using Eqs. (17)-(20). The results are presented in the Table 7.

Optics EXPRESS

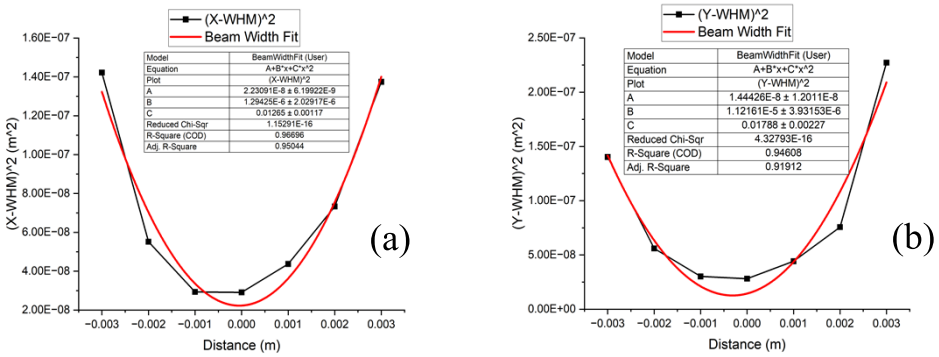

Fig. 15. The graph of the obtained points and the quadratic function fitted to them. For fitting, the Eq. (16) is defined for the software: (a) x-axis and (b) y-axis.

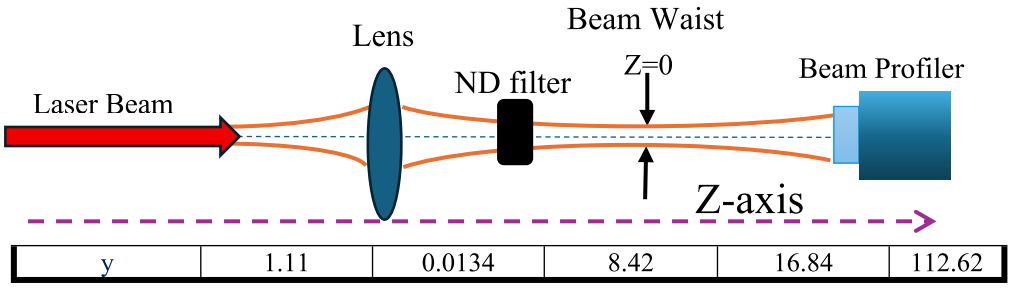

Fig. 16. The optical layout designed for the calculation of the laser beam quality and spot size.

Table 7. Parameters calculated by ISO method

Parameters	M^2	θ [rad]	Z_R[mm]	b[mm]	ω_0[μm]
x	1.24	0.0112	13.26	26.53	149.25
y	1.11	0.0134	8.42	16.84	112.62

The standard ISO method is not easy to practice, nor is it fast enough to make measurements. However, according to the results gained in this study, it can be considered appropriate for the measurement of beam quality. The obtained values $M_x^2 = 1.24$ *and* $M_y^2 = 1.11$ indicate that the laser beam generated in the ring cavity possesses very high quality. Figure 17 displays the beam profile obtained by the beam profiler software at z = 0, which, as evident, clearly demonstrates that the beam profile closely aligns with an ideal Gaussian distribution.

Optics EXPRESS

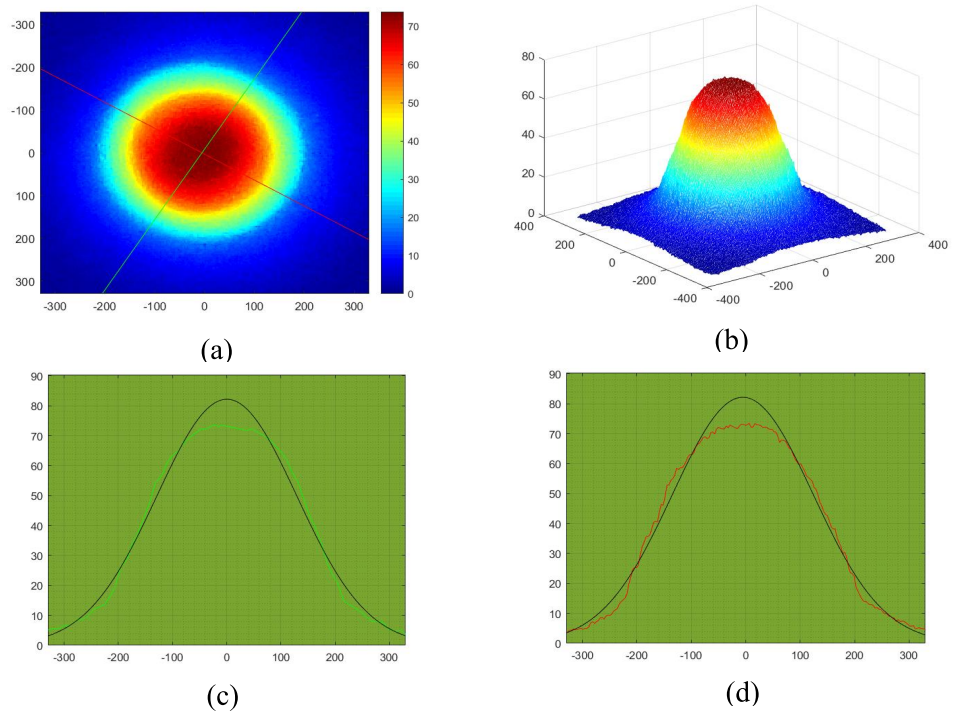

Fig. 17. The laser beam profile at z = 0, (a) 2D reconstruction of the beam profile, (b) the 3D profile. The intensity profiles of the laser beam and an ideal gaussian beam (black) vs radius (c) along the x axis (green) and (d) along the y axis (red).

7. Conclusion

In this work, we successfully designed, analyzed, and implemented a linearly polarized Nd:YAG laser using a novel coupled ring–linear cavity configuration under diode side-pumping. The integration of a side cavity incorporating a Brewster window effectively induced polarization selection, while redirecting part of the laser path back into the gain medium improved output power and suppressed power instabilities observed in conventional ring cavities.

Thermal lensing effects in the Nd:YAG crystal were systematically studied through both experimental measurements and LASCAD simulations, revealing strong agreement between the two approaches. This enabled accurate determination of cavity stability conditions and informed our optimization of resonator geometry. The system demonstrated excellent beam quality with an M^2 value close to 1, validating the effectiveness of our thermal and optical design. Compared to traditional designs, our configuration exhibited a 50% increase in output power, surpassing the 20–30% improvement reported by Bereczki and Wetter for dynamic ring resonators [2], and a significant enhancement in polarization purity, achieving up to 82% linear polarization efficiency, compared to 50–60% for traditional optical isolator methods [19].

Funding. Iran National Science Foundation (4039309).

Acknowledgment. This work is based upon research funded by Iran National Science Foundation (INSF) under project No 4039309. We express our sincere gratitude to INSF for their generous financial support, which was crucial for the successful completion of this research. The authors also thank Shahid Chamran University of Ahvaz for supporting this research.

Disclosures. The authors declare that they have no known competing financial interests or personal relationships that could have appeared to influence the work reported in this manuscript.

Optics EXPRESS

Data availability. Data underlying the results presented in this paper are not publicly available at this time but may be obtained from the authors upon reasonable request.

References

1. A. Bereczki and N. U. Wetter, "Dynamic stable ring resonator for high-power continuous single-frequency lasers: conditions for a compact resonator," Appl. Opt. **62**(8), C38–C42 (2023).
2. A. Bereczki, N.U. Wetter, and F.C. da Cruz, "Dynamically stable continuous single frequency green ring laser," In: *SBFoton International Optics and Photonics Conference (SBFoton IOPC), IEEE* (2019), pp. 1–4.
3. V. Magni, "Resonators for solid-state lasers with large-volume fundamental mode and high alignment stability," Appl. Opt. **25**(1), 107–117 (1986).
4. U. Keller, W. H. Knox, and H. Roskos, "Coupled-cavity resonant passive mode-locked Ti:sapphire laser," Opt. Lett. **15**(23), 1377–1379 (1990).
5. G.S. He, Y. Cui, G.C. Xu, *et al.*, "Multiple mode-locking of the Q-switched Nd: YAG laser with a coupled resonant cavity," Opt. Commun. **96**(4-6), 321–329 (1993).
6. A.D. Deleva, Z.I. Aneva, Z.Y. Peshev, *et al.*, "Injection seeding in a ring-linear dual-cavity tunable laser," In: *Tenth International School on Quantum Electronics: Laser Physics and Applications*, P. A. Atanasov and D. V. Stoyanov, eds. (1999), pp. 112–116
7. D. D'Agostino, D. Lenstra, H.P.M.M. Ambrosius, *et al.*, "Coupled cavity laser based on anti-resonant imaging via multimode interference," Opt. Lett. **40**(4), 653–656 (2015).
8. H. Cao and J. Wiersig, "Dielectric microcavities: Model systems for wave chaos and non-Hermitian physics," Rev. Mod. Phys. **87**(1), 61–111 (2015).
9. H.H.B. Sapingi, "Developing Coupled Cavity Living," Ph.D. dissertation (united kingdom, cardiff,2016).
10. B. Bahari, A. Ndao, F. Vallini, *et al.*, "Nonreciprocal lasing in topological cavities of arbitrary geometries," Science. **358**(6363), 636–640 (2017).
11. S. Ullah, S. Pian, F. Dai, *et al.*, "Q. Single-Mode Semiconductor Nanowire Lasers With Coupled Cavities," Front. Chem. **8**, (2021).
12. L. Gianfrani, S. M. Hu, and W. Ubachs, "Advances in cavity-enhanced methods for high precision molecular spectroscopy and test of fundamental physics," Riv. Nuovo Cim. **47**(4), 229–298 (2024).
13. T. P. Letsou, D. Kazakov, P. Ratra, *et al.*, "Hybridized Soliton Lasing in Coupled Semiconductor Lasers," Phys. Rev. Lett. **134**(2), 023802 (2025).
14. H. Y. Hammod and R. N. Ketan, "Employment of Lascad Program to Study the Thermal Distribution across Nd: Yag Disc Pumped by Diode Laser," MINAR Journal **4**(1), 1–138 (2022).
15. C. T. Wu, F. Chen, and Y. L. Ju, "A simple method to estimate the thermal focal length of LD-end-pumped Tm:YAG crystal at room temperature," Optik **126**(13), 1300–1302 (2015).
16. S. Tushar, S. Nath, J. Akhtar, *et al.*, "Modeling and Analysis of Z Folded Solid State Laser Cavity with Two Curved Mirrors," International Journal of Microwave and Optical Technology. **13**, 2018.
17. P.B. Bisht, "ABCD matrices and stability diagrams," In: *An Introduction to Photonics and Laser Physics with Applications (IOP)* (2022), pp. 11–18.
18. W. Koechner, *Solid-State Laser Engineering*, 6th ed. (Springer, 2006).
19. F.H. Cao, Y. Li, Y.F. Dong, *et al.*, "Based on the KTP crystal double frequency laser experiment system research," In: *2nd International Conference on Materials Engineering and Information Technology Applications (MEITA)* (2016), pp. 527–531.
20. M. Khabbaz, M. Sabaeian, S. M. Mousavi Ghahfarrokhi, *et al.*, "Preparation of blue-light diode lasers for pumping applications: cooling system, characterization, and beam shaping," J. Mod. Opt. **70**(11), 690–706 (2023).
21. E.S. Anthony, "New developments in laser resonators," Proc.SPIE **1224**, 2–14 (1990).
22. B. Saleh and M. Teich, *Fundamentals of Photonics*, 2nd ed. (Wiley, 2007).
23. "International Organization for Standardization. ISO 111 test methods for laser beam widths, divergence angles and beam propagation ratios– part 1: stigmatic and simple astigmatic beams / part 2: general astigmatic beams/part3:intrinsic and geometrical laser beam classiffication, propagation and details of test methods," Geneva: ISO11146-1:2005.